CHEMISTRY OF MATERIALS

Article

pubs.acs.org/cm

Facile Droplet-based Microfluidic Synthesis of Monodisperse IV–VI Semiconductor Nanocrystals with Coupled In-Line NIR Fluorescence Detection

Ioannis Lignos,[†] Loredana Protesescu,[‡,§] Stavros Stavrakis,[†] Laura Piveteau,[†,‡] Mark J. Speirs,[∥] Maria A. Loi,[∥] Maksym V. Kovalenko,[‡,§] and Andrew J. deMello*[,†]

[†]Institute for Chemical & Bioengineering, Department of Chemistry & Applied Biosciences, ETH Zürich, Vladimir-Prelog-Weg 1, 8093, Switzerland

[‡]Institute of Inorganic Chemistry, Department of Chemistry and Applied Biosciences, Vladimir-Prelog-Weg 1, 8093, Switzerland

[§]Empa-Swiss Federal Laboratories for Materials Science and Technology, Überlandstrasse 129, 8600, Switzerland

[∥]Zernike Institute for Advanced Materials, University of Groningen, Nijenborgh 4, 9747, Groningen, The Netherlands

Supporting Information

ABSTRACT: We describe the realization of a droplet-based microfluidic platform for the controlled and reproducible synthesis of lead chalcogenide (PbS, PbSe) nanocrystal quantum dots (QDs). Monodisperse nanocrystals were synthesized over a wide range of experimental conditions, with real-time assessment and fine-tuning of material properties being achieved using NIR fluorescence spectroscopy. Importantly, we show for the first time that real-time monitoring of the synthetic process allows for rapid optimization of reaction conditions and the synthesis of high quality PbS nanocrystals, emitting in the range of 765–1600 nm, without any post-synthetic processing. The segmented-flow capillary reactor exhibits stable droplet generation and reproducible synthesis of PbS nanocrystals with high photoluminescence quantum yields (28%) over extended periods of time (3–6 h). Furthermore, the produced NIR-emitting nanoparticles were successfully used in the fabrication of Schottky solar cells, exhibiting a power conversion efficiency of 3.4% under simulated AM 1.5 illumination. Finally, the droplet-based microfluidic platform was used to synthesize PbSe nanocrystals having photoluminescence peaks in the range of 860–1600 nm, showing the exceptional control and stability of the reactor.

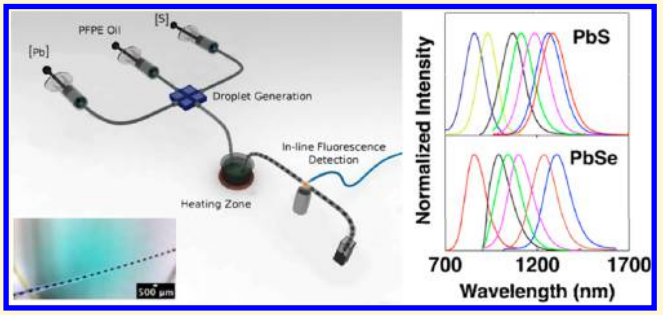

INTRODUCTION

The development of effective strategies for the controlled synthesis of near-infrared (NIR) active colloidal quantum dots (QDs, also known as semiconductor nanocrystals, NCs), with size-tunable emission and absorption spectra, remains a significant challenge.[1−4] III–V, II–VI and IV–VI type NIR QDs (including InAs, GaAs, PbS, PbSe, CdTe, HgTe)[3−5] exhibit superior fluorescence quantum yields and photostability when compared to conventional organic fluorophores that are commonly used in optoelectronic devices or *in vivo* imaging.[3] Of all such materials, lead sulfide (PbS) NCs are presently most intensely researched due to their utility in ultrasensitive photodetectors[6] and as the absorber material in solution-processed solar cells.[7−10]

In recent years, the use of microfluidic systems for processing fluid samples and performing complex chemical and biological experiments has become increasingly popular. Specifically, microfluidic reactors have become highly attractive environments for synthesizing QDs of exceptional quality.[11] The benefits of using microfluidic systems to synthesize nanomaterials are both numerous and compelling. First, the precise and rapid control of reaction temperature enables the rapid heating and cooling of reaction mixtures.[12] Second, the rapid and continuous mixing of liquid precursors via both passive and active methods ensures the formation of homogeneous reaction mixtures on a millisecond time scale.[13] Third, the ability to dynamically change reaction conditions such as reagent concentrations and reaction time allows for the complete characterization of the synthetic process in a time and cost efficient manner.[14] Last but not least, microfluidic reactors can be easily integrated with in-line, real-time detection systems to allow for the rapid and "intelligent" mapping of the reaction phase space. Indeed, such approaches have successfully been used in small molecule organic synthesis and chemical analysis.[15] In the current context, such integrated microfluidic systems provide a unique opportunity to produce nanomateri-

Received: March 4, 2014
Revised: March 28, 2014
Published: April 7, 2014

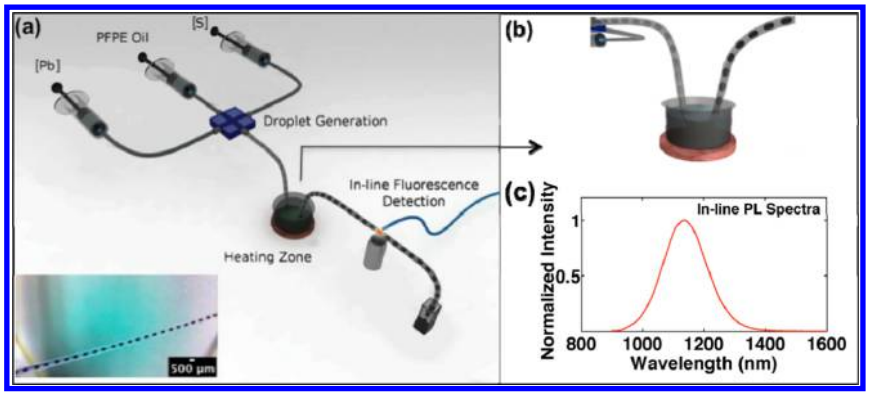

Figure 1. (a) Schematic of the droplet-based microfluidic reactor used for synthesis of PbS NC synthesis, including an in-line NIR fluorescence detection system. Bottom inset: Image of generated droplets containing synthesized PbS QDs. (b) Schematic of the color change of the generated droplets after transport through the heating section. (c) In-line PL characterization of the synthesized particles.

als[16−19] with defined chemical and physical properties. The in-line extraction of photoluminescence spectra allows rapid optimization of reaction conditions, thus avoiding material-consuming batch synthesis and post-synthetic processing that is the norm.

To date, both continuous- and segmented-flow microfluidic systems have been used to synthesize a variety of metal nanoparticles (NPs) and compound semiconductor NCs including Au,[20−22] Ag,[21,23] Co,[24,25] Pd,[26] SiO_2,[27,28] TiO_2,[29] Fe_2O_3,[30,31] CdS,[32] CdSe,[17,33] InP,[34] CdSe/ZnS,[35−37] and ZnSe/ZnS[38] of various sizes, shapes, and with narrow size distributions. In almost all situations, continuous flow microfluidic reactors generate higher quality products than corresponding batch (macroscale) reactors. However, issues related to Taylor dispersion and fluid interaction with the reactor walls limit their ultimate utility in nanocrystal synthesis.[39] In addition, reactor fouling is a practical issue hindering the use of continuous flow microfluidics in production settings. Such fouling at best will cause a time-dependent variation in fluid dynamics and at worst causes reactor failure through blockage.[40] Fortunately, all of these issues can be overcome to a large extent by adopting a droplet-based or segmented-flow microfluidic format.[12,14] Here, the reaction mixture is compartmentalized within discrete pL−nL (picoliter−nanoliter) volumes that reside within an immiscible carrier fluid.[14] Such compartmentalization ensures that there is no interaction between the reaction mixture and the channel surface. Key advantages of segmented-flow regimes further include rapid reagent mixing and the elimination of residence time distributions.[41] For example, Shestopalov et al. demonstrated a liquid−liquid segmented-flow approach for the aqueous synthesis of CdS and CdS/CdSe core−shell NCs in a polydimethylsiloxane (PDMS) microfluidic device.[42] The QDs were formed using a two-stage synthetic approach with mixing occurring on a millisecond time scale. Extending this synthetic approach, Chan et al. developed a droplet-based microfluidic glass reactor for the synthesis of CdSe QDs.[33] Droplets of Cd and Se precursors were generated within a perfluorinated carrier fluid at high temperatures (~300 °C) allowing the stable and reproducible formation of monodisperse NPs. More recently, Nightingale et al. reported a droplet-based capillary reactor for the preparation of CdSe and metal oxide NCs.[17] The authors demonstrated the controlled synthesis of NCs with in-line characterization over a wide range of temperatures and reaction times.

Despite significant advances in the synthesis of high quality QDs using segmented-flow microfluidics, the vast majority of case studies have focused on the formation of II−VI semiconductor NCs of controlled size, shape, and chemical composition.[11] Lead chalcogenide QDs, such as PbS, PbSe, and PbTe, are recognized to be interesting active candidates in a variety of applications, including solar cells,[10,43,44] photodectors,[45,46] NIR lasers,[47] and biological imaging.[48] Lead sulfide NCs are IV−VI semiconductor materials that possess small band gaps (~0.8−1.6 eV), along with stable and tunable emission in the NIR region and high luminescence quantum yields (typically between 10 and 40%).[1] A variety of macroscale "top-down"[49] and "bottom-up" strategies[50−52] have been shown to be successful in producing high-quality PbS and PbSe QDs. Of these, the hot injection method proposed by Hines and Scholes in 2001 still remains the most widely used method for obtaining near monodisperse and size-tunable PbS NCs (4−10 nm, with typical standard size deviations of 10−15%), with optical bandgaps in the range of 800 to 1800 nm.[50] Specifically, the reaction between lead(II) oleate and bis-(trimethylsilyl) sulfide (TMS_2S) in the presence of oleic acid (OA) and octadecene (ODE) is utilized. Alternative synthetic methods, using batch[53,54] and segmented flow reactors,[55] have also been established for the formation of PbS NCs. However, both lead to the formation of particles within a limited size range. Accordingly, a platform that combines the intrinsic advantages of droplet-based microfluidics and the rapid in-line characterization of the synthesized particles is needed for the production of IV−VI QDs with programmable chemical and physical characteristics. To this end, we report a one-stage approach for the synthesis of size-tunable and monodisperse lead chalcogenide NPs using a droplet-based capillary reactor. The capillary reactor is able to generate highly monodisperse droplets for the fast mixing of precursor solutions. Moreover, we show for the first time that the photoluminescence of the synthesized PbS and PbSe QDs can be monitored in real-time through the use of an in-line fluorescence spectrometer, which facilitates the rapid screening of a wide range of experimental conditions on short time scales. Through adaptation of the reaction system reported by Hines et al. and application of direct sample heating,[50] PbS NCs with narrow size distributions (5−7%) and band edge emission between 765 and 1580 nm are produced in an efficient manner. To ensure both size-tunability and low size-dispersion a wide range of temperatures (80−155 °C), reaction times (3−30 s), and OA/ODE concentration

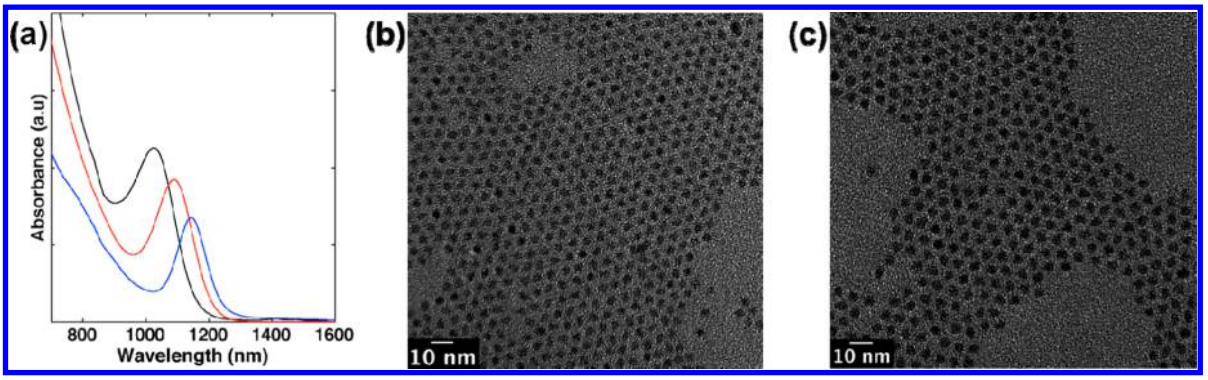

Figure 2. (a) Absorption spectra of PbS QDs synthesized in a droplet-based capillary reactor. Black line: R.t = 15 s, T = 125 °C, Pb/S = 1, ODE/OA = 5.67. Red line: R.t = 11 s, T = 130 °C, Pb/S = 1, ODE/OA = 5.67. Blue line: R.t = 14 s, T = 135 °C, Pb/S = 1, ODE/OA = 5.67. (b,c) TEM micrographs of 3.8 ± 0.2 nm (R.t = 6 s, T = 145 °C, Pb/S = 1, ODE/OA = 3, Q_{Galden} = 95 μL/min, Q_{Pb} = Q_S = 30 μL/min) and 4.5 ± 0.3 nm (R.t = 11 s, T = 150 °C, Pb/S = 1, ODE/OA = 3, Q_{Galden} = 70 μL/min, Q_{Pb} = Q_S = 20 μL/min) PbS NCs synthesized in droplets of ODE in Galden.

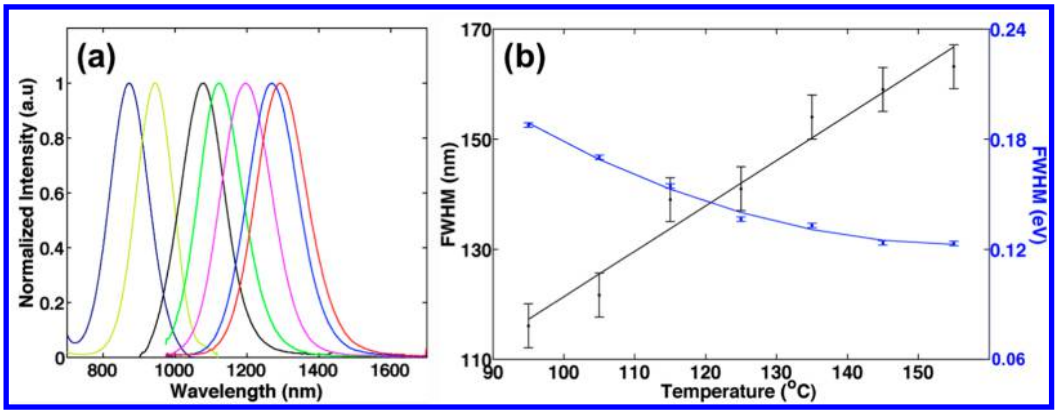

Figure 3. In-line photoluminescence spectra of the PbS QDs synthesized by the droplet-based capillary reactor. Tuning of (a) the PL peak position and (b) FWHM in nm and eV with temperature (T = 95−155 °C, increasing by 10 °C), holding the reaction time at 11 s, the Pb/S ratio equal to 1, and the ODE/OA ratio at 5.67 (the total flow rate (Q) is constant at Q_{Galden} = 50 μL/min, Q_{Pb} = Q_S = 20 μL/min).

ratios were explored. Importantly, our approach allows the reproducible synthesis of ultrasmall QDs, having PL peaks in the range of 765−850 nm. Finally, the droplet-based capillary reactor was successfully applied to the synthesis of monodisperse PbSe QDs with photoluminescence emission in the range of 860−1600 nm.

■ RESULTS AND DISCUSSION

PbS QD Synthesis and Characterization. The capillary droplet-based reactor shown in Figure 1a consists of a cross configuration for generating nanoliter droplets followed by a 10−15 cm segment of PTFE tubing (ID = 500 μm, OD = 1/16″) immersed in an oil bath. Three separate syringes feed the two precursor solutions (Pb and S) and the carrier fluid through the cross connector. A rapid color change (colorless to brown) of the bulk droplets suggests an equally rapid reaction between the Pb and S precursors (Figure 1b). As the droplets exit the oil bath (Figure S1), they are optically excited using a 625 nm light emitting diode (LED). Time-integrated fluorescence spectra (Figure 1c) from individual droplets are then measured using a homemade fiber-based spectrometer, with full spectrum acquisition of 100 ms. Finally samples are collected at the outlet of the tubing in vials and cooled in an ice bath.

Our microfluidic system allows for the generation of monodisperse droplets or slugs (Figure 1a, bottom inset) over a wide range of flow rates and temperatures. Our integrated fluorescence detection system enables the optimization of particle characteristics through variation of temperature, reaction time (R.t.) and precursor/surfactant/solvent ratios (Figure 2a). The narrow size distribution and the shape-uniformity of the synthesized PbS QDs were further confirmed by Transmission Electron Microscopy (TEM) imaging (Figure 2b,c). The particles have diameters of 3.8 ± 0.2 nm and 4.5 ± 0.3 nm, respectively (see Figure S2 for corresponding size distribution histograms; Figures S3 and S4 demonstrate X-ray diffraction and Fourier transform infrared spectroscopy diagrams, respectively).

Figure 3a demonstrates how particle emission can be tuned by systematic variation of the operating temperature while all other reaction conditions are fixed (R.t = 11 s, ODE/OA = 5.67, Pb/S = 1). Increasing the temperature at a constant residence time results in the shift of the band edge emission to longer wavelengths, due to the production of larger particles,[17,33] and a broadening (Figure 3b) of the band edge emission linewidth. Both observations suggest that the growth of PbS NCs follows the same reaction model demonstrated in CdSe and PbSe synthesis.[56,57] Analyzing the behavior of the emission linewidth in terms of energy (Figure 3b, blue line), it is observed that the full width at half maximum (FWHM) varies between 0.12 and 0.19 eV. Generally, reactions carried out at temperatures over 155 °C result in broad size distributions (see Supporting Information, Figure S5) due to the formation of nonspherical PbS particles.[58] Moreover, it is

dx.doi.org/10.1021/cm500774p | Chem. Mater. 2014, 26, 2975−2982

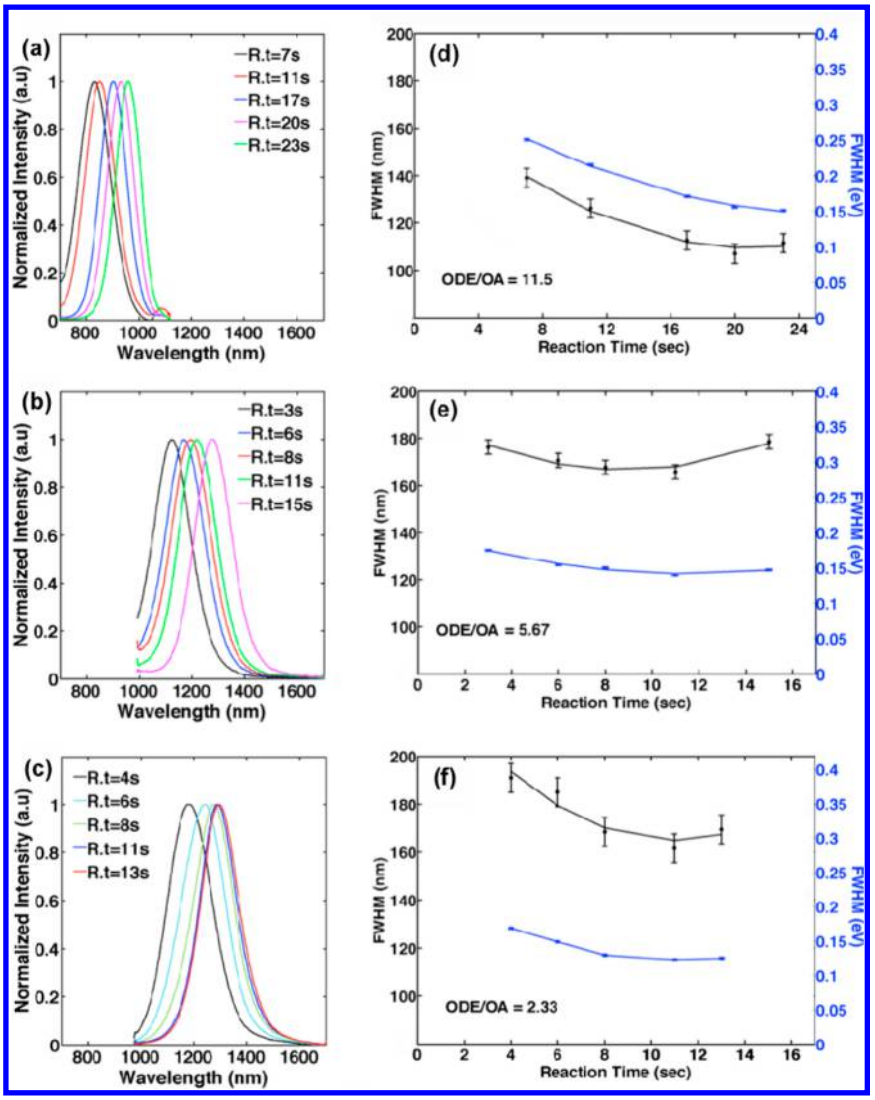

Figure 4. In-line fluorescence characterization of PbS QDs synthesized in a droplet-based capillary reactor at 135 °C (Pb/S = 1). (a–c) Tuning of the PL spectra and (d,e) FWHM variation in nm and eV with the reaction temperature and the ODE/OA ratio.

striking to note that syntheses at temperatures below 85 °C provide for the controlled synthesis of ultrasmall PbS QDs with PL peaks in the range of 750–800 nm (see Figures S6 and S7).

The effect of the reaction time on PbS QD size was investigated by varying the flow rates of the individual input streams. In all cases, the reaction temperature was maintained at 135 °C. Inspection of Figure 4a demonstrates that the PL peak shifts to longer wavelengths as the reaction time is increased from 7 to 23 s, at a constant ODE/OA ratio of 11.5. Furthermore, it is observed that the formed PbS NCs are relatively small with PL emission in the range of 850–930 nm. Nevertheless, it can be seen that the reaction time has a weaker influence on the PL peak than the operating temperature. Previous studies on PbS synthesis suggest that low ODE/OA ratios favor the formation of large PbS NCs of about 6.5 nm in diameter.[50] Figure 4b and c show the variation of the excitonic peak as the ODE/OA ratio is decreased from 5.67 to 2.33 respectively. Such a variation allows control of the band edge emission between 1050 and 1300 nm. Increasing the reaction time (Figure 4d) initially causes particle self-focusing, (i.e., the FWHM of the band edge emission decreases), followed by a tendency toward size broadening. The same behavior is observed for all three ODE/OA ratios (Figure 4e,f). This trend can be explained using colloidal growth theory developed by Peng et al.[59] Here, size focusing occurs when the nanocrystal diameter is larger than a critical size. Under these conditions, small particles grow faster than larger particles. However, after depletion of molecular precursors the critical diameter shifts to a value larger than the average particle size present. This causes "size broadening" of the synthesized NCs, since large particles continue to grow while small particles shrink. In addition, an ODE/OA ratio <1.33 leads to the formation of PbS particles emitting between 1300–1600 nm with broad size distributions. Using a continuous flow approach, NCs with narrow size distributions and a band edge emission between 1300 and 1580 nm are obtained (Figure S9).

The effect of reaction time on particle characteristics was further explored by performing the synthesis at four different temperatures, while keeping all other experimental conditions constant (ODE/OA = 5.67, Pb/S = 1). It is noticeable from Figure 5 that the droplet-based reactor functions with precise control over a range of different reaction conditions. The red-shift in the band edge emission as a function of residence time is evident for all tested temperatures. In addition, the excellent

dx.doi.org/10.1021/cm500774p | Chem. Mater. 2014, 26, 2975–2982

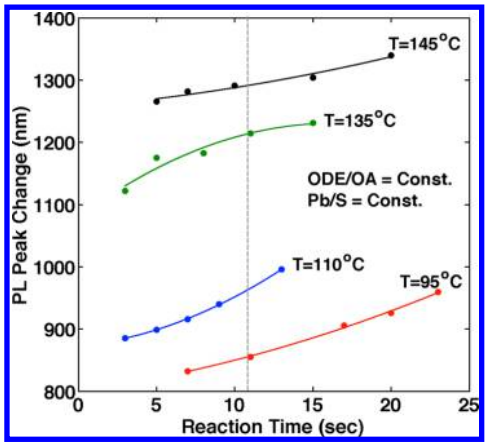

Figure 5. Variation of peak emission wavelength as a function of reaction time at different operating temperatures (95, 110, 135, and 145 °C. In each case, the ODE/OA ratio and the Pb/S ratio equal 5.67 and 1, respectively. The reproducibility of the PL peak position using the droplet-based reactor is confirmed through use of the 11 s residence time experiment (dashed line). The projected wavelengths are in agreement with those acquired in Figure 2a.

reproducibility in synthesized particle size is apparent for a residence time of 11 s (Figure 5, dashed line), where the obtained PL data, from four different series of measurements, are identical to those presented in Figure 3a for the same experimental conditions.

To assess the stability and reproducibility of the microfluidic reactor, a long-term evaluation of photoluminescence characteristics of the produced particles was conducted, where reaction conditions were kept constant (Figure 6a) for a period of 3 h (see Figure S11 for additional stability tests). The PL spectra (Figure 6a) and variation of the emission peak wavelength and FWHM (Figure 6b) were recorded as a function of time. It can be seen that the PL peak is essentially invariant around 1308 ± 11 nm with a FWHM of 158 ± 6 nm over this period. The small variations from the mean value are attributed to

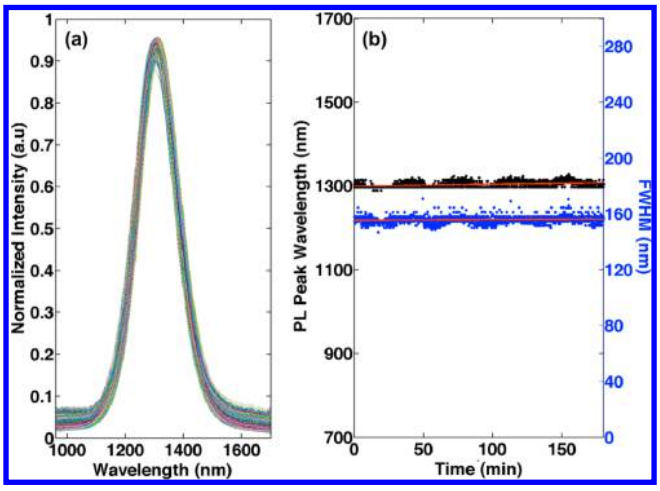

Figure 6. Long-term stability measurements of the PbS quantum dot formation in a droplet-based reactor. (a) Emission spectra and (b) PL peak and FWHM variation over 3 h of continuous operation. The reaction conditions were fixed at R.t = 11 s, T = 135 °C, ODE/OA = 3, Pb/S = 1, Q_{Galden} = 70 μL/min, Q_{Pb} = Q_S = 20 μL/min. For longer reactor operation with the same experimental conditions, syringe refilling is required.

fluctuations in the temperature of the heating bath from the set point (±1 °C).

Furthermore, the superior quality of the synthesized QDs was confirmed by measurement of fluorescence quantum yields, which were up to 28% (with respect to infrared dye−IR-26[60] in 1,2-dichloroethane) for PbS QDs, synthesized in our droplet-based microfluidic system.[54,61] The measured fluorescence quantum yields for particles synthesized in our microfluidic reactors are significantly higher than fluorescence quantum yield values obtained from batch-synthesized NCs (which yield values between 7 and 12%; Table S1 and S2). In addition, the NIR-emitting NCs were successfully used to fabricate Schottky-type solar cell devices. The photovoltaic devices consist of a PbS nanocrystal layer sandwiched between an indium tin oxide (ITO) and a LiF/Al electrode. The fabricated devices were shown to function with an excellent efficiency of 3.4% with short-circuit current J_{sc} = 13.9 mA cm^{-2} and an open-circuit voltage V_{oc} = 0.45 V (Figure S14).

PbSe QD Synthesis and Characterization. To demonstrate the broader applicability of the droplet-based microfluidic reactor for the synthesis of IV−VI colloidal QDs, we finally describe the controlled formation of PbSe NCs. Since PbSe QDs are not air-stable,[62,63] it was necessary to flush all tubing with N_2 for several minutes and de-gas the oil phase prior to each experiment. Adapting the reaction system suggested by Talapin and Murray[64] and applying the same synthetic procedure we describe for the synthesis of PbS NCs, we performed the synthesis of PbSe QDs. By a systematic variation of the operating temperature and keeping all the other experimental parameters fixed (R.t = 70 s, Squalene/OA = 5.67, Pb/Se = 1), we successfully formed monodisperse PbSe NCs (Figure 7a) with an optical bandgap that varies between 860 and 1300 nm (PbSe particles emitting in the range of 1300−1600 nm were also synthesized, see Figure S15). TEM images (Figure S16) confirm the narrow size distribution of the synthesized PbSe particles. Comparing the PL peak shift of the synthesized PbS and PbSe QDs as a function of temperature (Figure 7b), it is apparent that temperature variation has a stronger influence on the emission peak wavelengths of the synthesized PbSe particles than those of PbS QDs. However, PbS particles emitting in the range of 800−1400 nm are formed at a much faster rate (R.t = 11 s) than PbSe NCs (R.t = 70 s) under the same operating temperature.

CONCLUSIONS

We have demonstrated a controlled droplet-based microfluidic platform for the synthesis of monodisperse PbS and PbSe QDs under a wide range of experimental conditions and with rapid in-line photoluminescence characterization. The synthesized particles have narrow size distributions, in the range of 5−7%. The process control and optimization of reactions were achieved via *in situ* monitoring of photoluminescence from individual droplets. Notably, the synthesized PbS QDs, emitting between 765 and 1580 nm, exhibit significantly higher quantum efficiencies (∼28%) than those synthesized using conventional macroscale reactors (∼12%). Reactor operation over long periods (3−6 h) of time further confirms the stability of our droplet generation and the precise control over particle formation. In addition, PbS-based Schottky solar cells were fabricated using the synthesized particles, which demonstrated excellent power efficiencies in excess of 3%. Moreover, the synthesis and size tuning of monodisperse PbSe particles, with an optical bandgap in the range of 860−1600 nm, ensures the

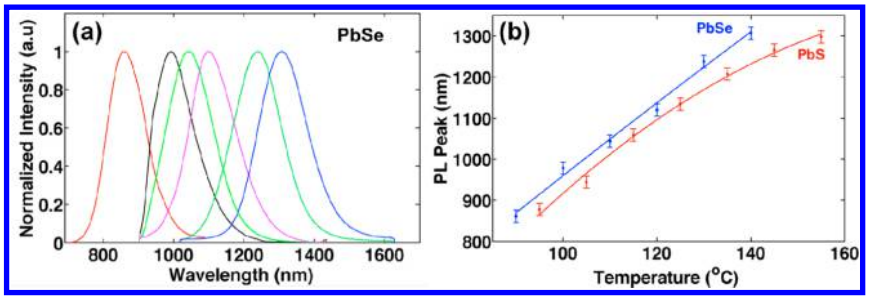

Figure 7. In-line photoluminescence spectra of the PbSe QDs synthesized by the droplet-based capillary reactor. (a) Tuning of the PL peak position (T = 90−140 °C, increasing by 10 °C), holding the reaction time at 70 s, the Pb/Se ratio equal to 1, and the Squalene/OA ratio at 5.67 (the total flow rate is constant at Q_{Galden} = 70 μL/min, Q_{Pb} = Q_S = 20 μL/min). (b) Comparison of the peak wavelength shift of the PbS and PbSe QDs as a function of temperature ($R.t_{PbSe}$ = 70 s, $R.t_{PbS}$ = 11 s).

versatility of the droplet-based capillary reactor. Adoption of the proposed methodology allows for high-throughput kinetic measurements with millisecond time resolution for systems with very short nucleation and/or growth times, which are typically performed using the hot-injection method (Cd, Pb, and non-heavy metal chalcogenides, as an example). Finally, process scale-out can efficiently accelerate the production of a wide range of NIR emitting nanomaterials with narrow size distributions at a gram to kilogram per day production level.

METHODS

Materials. Lead(II) acetate trihydrate ($Pb(CH_3CO_2)_2{\cdot}3H_2O$, ≥99.99%, powder), bis(trimethylsilyl)sulfide (TMS_2S, synthetic grade), selenium (Se, 95%, powder), oleic acid (OA, 90%), 1-octadecene (ODE, 90%), squalene (99+%), trioctylphosphine (TOP, 97%), ethanol over molecular sieve ($H_2O \leq 0.01\%$), and *n*-hexane absolute over molecular sieve ($H_2O \leq 0.01\%$) were purchased from Sigma-Aldrich and used as received. Toluene anhydrous (99.8%) and tetracholoroethylene (99%) were purchased from ABCR-Chemicals. Galden PFPE was purchased from Blaser Swisslube AG.

Preparation of Precursors. *PbS Synthesis.* In a three-neck flask, $PbAc_2{\cdot}3H_2O$ (1 mmol, 0.379 g), ODE (5−9 mL), and OA (5−1 mL) were dried at 120 °C under a vacuum for 2 h to dissolve the lead salt and dry the solution. The solution was then allowed to cool before being loaded into a 10 mL gastight glass syringe (Hamilton). In a glovebag (Sigma-Aldrich), the sulfur precursor solution was prepared by mixing TMS_2S (210 μL, 1 mmol) with ODE (20 mL). The solution was then loaded in a 10 mL gastight glass syringe. The Galden continuous phase was loaded in a 25 mL gastight glass syringe (Hamilton).

PbSe Synthesis. In a three-neck flask, $PbAc_2{\cdot}3H_2O$ (1.2 mmol, 0.456 g), squalene (7.5−8.5 mL), and OA (1.5−2.5 mL) were dried at 120 °C under a vacuum for 2 h to dissolve the lead salt and dry the solution. The solution was then allowed to cool before being loaded into a 10 mL gastight glass syringe (Hamilton). In a glovebox, the selenium precursor solution was prepared by dissolving Se (9 mmol, 0.711 g) in TOP (9 mL). The solution was then loaded in a 10 mL gastight glass syringe. The Galden continuous phase was degassed prior to each experiment, and then it was loaded in a 25 mL gastight glass syringe (Hamilton).

Construction of the Microfluidic Reactor. PTFE tubing (ID 250 μm) was attached to the glass syringes using polyether ether ketone (PEEK) luer-lock interconnects (Upchurch Scientific) and on the other end to a PEEK cross (Upchurch). PTFE tubing (30 cm, OD 1/16″, ID 500 μm) was also attached to the PEEK cross and immersed in an oil bath. A PEEK union (Upchurch) was used to connect the PTFE tubing with high-purity PFA tubing (OD 1/16″, ID 500 μm) for fluorescence measurements.

Synthesis and In-line Characterization of PbS QDs. In a typical experiment, Nemesys precision syringe pumps were used to inject dispersed and carrier fluids into a PEEK cross at different (Pb+S)/Galden flow rate ratios. A section (10−60 cm) of PTFE tubing was immersed in the oil bath where the set point temperatures ranged from 80 to 155 °C. For PbSe QD synthesis, the microfluidic reactor was flashed with N_2 since PL spectra of the synthesized particles are very sensitive to residual air inside the tubing. The generated droplets were heated inside the oil bath and the reaction time calculated by measuring the time that it takes for individual droplets to traverse the heated segment. Droplets containing synthesized QDs were then cooled to 25 °C and motivated into the in-line NIR optical system. In-line NIR fluorescence spectroscopy was performed by exciting individual droplets using a 625 nm Light Emitting Diode (LED, M625L3 Thor Labs), with emission being captured by a fiber-optic coupled InGaAs array spectrometer (Sol 1.7, 900−1700 nm, BWTEK). Emission spectra in the range of 700−950 nm were recorded using a fiber-optic coupled CCD Spectrometer (QE65 Pro, 200−1100 nm, Ocean Optics). All recorded spectra were analyzed using a homemade Matlab script. The reaction product was collected from the end of the PFA tubing in a vial on top of an ice bath.

Offline QD Characterization. PbS particles were washed in air using anhydrous solvents. On the other hand, PbSe particles were washed in an inert atmosphere. Hexane (300 μL) and ethanol (300 μL) were added to the crude solution followed by centrifugation to separate the QDs from the organic ligands. Obtained PbS QDs were redispersed in hexane and again precipitated with ethanol for two additional washing steps and then redispersed in 300 μL of toluene. Samples were then dried under a vacuum to remove toluene and redispersed in tetrachloroethylene (TCE) for absorption and photoluminescence measurements. Absorption spectra of the synthesized NCs were collected using a Cary 5000 UV−vis−NIR spectrometer. Offline photoluminescence measurements were conducted in a homemade setup using a cuvette holder with four light ports and optical fibers. For fluorescence quantum yield measurements, all samples were excited at 960 nm. Measured intensities were corrected to account for the spectral response of the spectrometer. Infrared dye IR-26 (Exciton Inc.) dissolved in 1,2-dichloroethane was used as a fluorescence reference with recently corrected absolute fluorescence quantum yields by Semonin et al.[60] To obtain fluorescence quantum yields for PbS NCs in colloidal solution, integrated luminescence intensities were directly compared to that of IR-26 dye, taking into account the optical density at the excitation wavelength. To avoid reabsorption of emitted light, the optical density of the PbS sample at the excitation wavelength was kept below 0.1. Transmission electron microscopy of the samples was carried out using a FEI Tecnai F30 microscope operating at 300 kV.

Schottky Solar Cell Fabrication. The washing procedure for the preparation of PbS QDs for solar cell devices was performed as follows: hexane (10 mL) and ethanol (10 mL) were added to the crude solution followed by centrifugation to separate QDs from the organic ligands. The PbS QDs were then redispersed in hexane (10 mL) and precipitated again with ethanol (10 mL). After another washing cycle with ethanol/hexane, the particles were redispersed in chloroform (5 mL). A part of this solution was further precipitated from chloroform with methanol (15 mL) and then redispersed in chloroform.

PbS QDs were deposited onto a prepatterned ITO substrate using an iterated two-step method consisting of spin-coating and subsequent replacement of the OA ligands with 1,4-benzenedithiol. The total active layer of 140 nm thicknesses was thermally annealed at 140 °C. The device was finished by thermal evaporation of LiF (1 nm) and Al (100 nm) layers.

Current−voltage characteristics were recorded using a Keithley 2400 Source Meter with the device kept in a nitrogen glovebox. Measurements were performed in the dark and under illumination from a Steuernagel Solar Constant 1200 metal halide lamp calibrated to 1 sun intensity and corrected for spectral mismatch with an air mass (AM) 1.5G spectrum using a Si reference cell. Contributions to the photocurrent from regions outside the anode/cathode overlap area were eliminated using a mask with a slightly smaller aperture than the device area.

■ ASSOCIATED CONTENT

Ⓢ Supporting Information

TEM images, PL emission spectra, size distribution diagrams, current density−voltage characteristics. This material is available free of charge via the Internet at http://pubs.acs.org.

■ AUTHOR INFORMATION

Corresponding Author

*E-mail: andrew.demello@chem.ethz.ch.

Funding

The work was partially supported by the Swiss National Science Foundation grant (200021_143638).

Notes

The authors declare no competing financial interests.

■ ACKNOWLEDGMENTS

We thank Dr. M. Bodnarchuk for the TEM micrographs and Y. Ding for the schematic illustration of the experimental setup.

■ REFERENCES

(1) van Veggel, F. C. J. M. *Chem. Mater.* **2013**, *26*, 111−122.
(2) Yin, Y.; Alivisatos, A. P. *Nature* **2004**, *437*, 664−670.
(3) Ma, Q.; Su, X. *Analyst* **2010**, *135*, 1867−1877.
(4) Talapin, D. V.; Lee, J.-S.; Kovalenko, M. V.; Shevchenko, E. V. *Chem. Rev.* **2010**, *110*, 389−458.
(5) Lhuillier, E.; Keuleyan, S.; Liu, H. *Chem. Mater.* **2013**, *25*, 1272−1282.
(6) Sargent, E. *Nat. Nanotechnol.* **2012**, *7*, 349−350.
(7) Ip, A. H.; Thon, S. M.; Hoogland, S.; Voznyy, O.; Zhitomirsky, D.; Debnath, R.; Levina, L.; Rollny, L. R.; Carey, G. H.; Fischer, A.; Kemp, K. W.; Kramer, I. J.; Ning, Z.; Labelle, A. J.; Chou, K. W.; Amassian, A.; Sargent, E. H. *Nat. Nanotechnol.* **2012**, *7*, 577−582.
(8) Kramer, I. J.; Sargent, E. H. *Chem. Rev.* **2013**, *114*, 863−882.
(9) Ning, Z.; Ren, Y.; Hoogland, S.; Voznyy, O.; Levina, L.; Stadler, P.; Lan, X.; Zhitomirsky, D.; Sargent, E. H. *Adv. Mater.* **2012**, *24*, 6295−6299.
(10) Piliego, C.; Protesescu, L.; Bisri, S. Z.; Kovalenko, M. V.; Loi, M. A. *Energy Environ. Sci.* **2013**, *6*, 3054−3059.
(11) Nightingale, A. M.; Demello, J. C. *Adv. Mater.* **2013**, *25*, 1806−1806.
(12) Elvira, K. S.; Solvas, X. C. I.; Wootton, R. C. R.; deMello, A. J. *Nat. Chem.* **2013**, *5*, 905−915.
(13) Hessel, V.; Löwe, H.; Schönfeld, F. *Chem. Eng. Sci.* **2005**, *60*, 2479−2501.
(14) deMello, A. J. *Nature* **2006**, *442*, 394−402.
(15) Yue, J.; Schouten, J. C.; Nijhuis, T. A. *Ind. Eng. Chem. Res.* **2012**, *51*, 14583−14609.
(16) Krishnadasan, S.; Brown, R. J. C.; deMello, A. J.; deMello, J. C. *Lab Chip* **2007**, *7*, 1434−1441.
(17) Nightingale, A. M.; Krishnadasan, S. H.; Berhanu, D.; Niu, X. *Lab Chip* **2011**, *11*, 1221−1227.
(18) Marre, S.; Baek, J.; Park, J.; Bawendi, M. G.; Jensen, K. F. *Jala* **2009**, *14*, 367−373.
(19) Knauer, A.; Koehler, J. M. *Nanotechnol. Rev.* **2013**, *3*, 5−26.
(20) Duraiswamy, S.; Khan, S. A. *Small* **2009**, *5*, 2828−2834.
(21) Lazarus, L. L.; Riche, C. T.; Marin, B. C.; Gupta, M.; Malmstadt, N.; Brutchey, R. L. *ACS Appl. Mater. Interfaces* **2012**, *4*, 3077−3083.
(22) Sebastian Cabeza, V.; Kuhn, S.; Kulkarni, A. A.; Jensen, K. F. *Langmuir* **2012**, *28*, 7007−7013.
(23) He, S. T.; Liu, Y. L.; Maeda, H. *J. Nanopart. Res.* **2008**, *10*, 209−215.
(24) Song, Y.; Modrow, H.; Henry, L. L.; Saw, C. K. *Chem. Mater.* **2006**, *18*, 2817−2827.
(25) Song, Y.; Henry, L. L.; Yang, W. *Langmuir* **2009**, *25*, 10209−10217.
(26) Kim, Y. H.; Zhang, L.; Yu, T.; Jin, M.; Qin, D.; Xia, Y. *Small* **2013**, *9*, 3462−3467.
(27) Khan, S. A.; Günther, A.; Schmidt, M. A.; Jensen, K. F. *Langmuir* **2004**, *20*, 8604−8611.
(28) Wacker, J. B.; Lignos, I.; Parashar, V. K.; Gijs, M. *Lab Chip* **2012**, *12*, 3111−3116.
(29) Milo, S. P. *Lab Chip* **2007**, *7*, 167−169.
(30) Abou-Hassan, A.; Bazzi, R.; Cabuil, V. *Angew. Chem., Int. Ed.* **2009**, *48*, 7180−7183.
(31) Kumar, K.; Nightingale, A. M.; Krishnadasan, S. H. *J. Mater. Chem.* **2012**, *22*, 4704−4708.
(32) Edel, J. B.; Fortt, R. *Chem. Commun.* **2002**, 1136−1137.
(33) Chan, E. M.; Alivisatos, A. P.; Mathies, R. A. *J. Am. Chem. Soc.* **2005**, *127*, 13854−13861.
(34) Baek, J.; Allen, P. M.; Bawendi, M. G.; Jensen, K. F. *Angew. Chem.* **2010**, *123*, 653−656.
(35) Wang, H.; Li, X.; Uehara, M.; Yamaguchi, Y. *Chem. Commun.* **2004**, 48−49.
(36) Wang, H. Z.; Nakamura, H.; Uehara, M.; Yamaguchi, Y.; Miyazaki, M.; Maeda, H. *Adv. Funct. Mater.* **2005**, *15*, 603−608.
(37) Luan, W.; Yang, H.; Fan, N.; Tu, S.-T. *Nanoscale Res. Lett.* **2008**, *3*, 134−139.
(38) Kwon, B.-H.; Lee, K. G.; Park, T. J.; Kim, H.; Lee, T. J.; Lee, S. J.; Jeon, D. Y. *Small* **2012**, *8*, 3257−3262.
(39) Teh, S.-Y.; Lin, R.; Hung, L.-H.; Lee, A. P. *Lab Chip* **2008**, *8*, 198−220.
(40) Krishnadasan, S.; Tovilla, J.; Vilar, R.; deMello, A. J.; deMello, J. C. *J. Mater. Chem.* **2004**, *14*, 2655.
(41) Song, H.; Chen, D. L.; Ismagilov, R. F. *Angew. Chem., Int. Ed.* **2006**, *45*, 7336−7356.
(42) Shestopalov, I.; Tice, J. D.; Ismagilov, R. F. *Lab Chip* **2004**, *4*, 316−321.
(43) Luther, J. M.; Law, M.; Beard, M. C.; Song, Q.; Reese, M. O.; Ellingson, R. J.; Nozik, A. J. *Nano Lett.* **2008**, *8*, 3488−3492.
(44) Sargent, E. H. *Nat. Photonics* **2009**, *3*, 325−331.
(45) Konstantatos, G.; Howard, I.; Fischer, A.; Hoogland, S. *Nature* **2006**, *442*, 180−183.
(46) Szendrei, K.; Cordella, F.; Kovalenko, M. V. *Adv. Mater.* **2009**, *21*, 683−687.
(47) Hoogland, S.; Sukhovatkin, V.; Howard, I.; Cauchi, S. *Opt. Express* **2006**, *14*, 3273−3281.
(48) Cao, J.; Zhu, H.; Deng, D.; Xue, B.; Tang, L. *Mater. Res. Part A* **2012**, *100A*, 958−968.
(49) Yang, J.; Ling, T.; Wu, W. T.; Liu, H.; Gao, M. R.; Ling, C. *Nature* **2013**, *4*, 1695.
(50) Hines, M. A.; Scholes, G. D. *Adv. Mater.* **2003**, *15*, 1844−1849.
(51) Cademartiri, L.; Bertolotti, J.; Sapienza, R.; Wiersma, D. S.; von Freymann, G.; Ozin, G. A. *J. Phys. Chem. B* **2006**, *110*, 671−673.
(52) Zhang, J.; Gao, J.; Miller, E. M.; Luther, J. M.; Beard, M. C. *ACS Nano* **2014**, *8*, 614−622.
(53) Bakueva, L.; Gorelikov, I.; Musikhin, S.; Zhao, X. S.; Sargent, E. H.; Kumacheva, E. *Adv. Mater.* **2004**, *16*, 926−929.

(54) Zhang, D.; Song, J.; Zhang, J.; Wang, Y.; Zhang, S.; Miao, X. *CrystEngComm* **2013**, *15*, 2532−2536.
(55) Pan, J.; El-Ballouli, A. O.; Rollny, L.; Voznyy, O.; Burlakov, V. *ACS Nano* **2013**, *7*, 10158−10166.
(56) Liu, H.; Owen, J. S.; Alivisatos, A. P. *J. Am. Chem. Soc.* **2007**, *129*, 305−312.
(57) Rempel, J. Y.; Bawendi, M. G. *J. Am. Chem. Soc.* **2009**, *131*, 4479−4489.
(58) Lee, S. M.; Jun, Y.; Cho, S. N.; Cheon, J. *J. Am. Chem. Soc.* **2002**, *124*, 11244−11245.
(59) Peng, X.; Wickham, J.; Alivisatos, A. P. *J. Am. Chem. Soc.* **1998**, *120*, 5343−5344.
(60) Semonin, O. E.; Johnson, J. C.; Luther, J. M. *J. Phys. Chem. Lett.* **2010**, *1*, 2445−2450.
(61) Moreels, I.; Justo, Y.; De Geyter, B.; Haustraete, K.; Martins, J. C.; Hens, Z. *ACS Nano* **2011**, *5*, 2004−2012.
(62) Moreels, I.; Fritzinger, B.; Martins, J. C. *J. Am. Chem. Soc.* **2008**, *130*, 15081−15086.
(63) Dai, Q.; Wang, Y.; Zhang, Y.; Li, X.; Li, R.; Zou, B.; Seo, J. T. *Langmuir* **2009**, *25*, 12320−12324.
(64) Talapin, D. V.; Murray, C. B. *Science* **2005**, *310*, 86−89.